Supporting Information

Combination of changeable π-conjugation and hydrophilic groups for developing water-soluble small molecular NIR-II fluorogenic probes

Xiaofan Zhang,‡[ab] Shili Shen,‡[ac] Diankai Liu,[a] Xiaohua Li,*[a] Wen Shi[a] and Huimin Ma*[ab]

[a] Beijing National Laboratory for Molecular Sciences, Key Laboratory of Analytical Chemistry for Living Biosystems, Institute of Chemistry, Chinese Academy of Sciences, Beijing 100190, China.

E-mail: lixh@iccas.ac.cn; mahm@iccas.ac.cn

[b] University of Chinese Academy of Sciences, Beijing 100049, China.

[c] School of Chemistry and Pharmaceutical Engineering, Shandong First Medical University & Shandong Academy of Medical Sciences, Tai'an, Shandong, 271016, China.

‡ These authors contributed equally to this work.

Contents

1. Experimental methods

Reagents. Unless otherwise specified, all reagents were purchased from J&K Scientific Ltd. or Beijing InnoChem Science & Technology Co., Ltd., and used as received. Leucine aminopeptidase (LAP) was purchased from Shanghai Yingxin Laboratory. Bestatin, 3-(4,5-dimethyl-2-thiazolyl)-2,5-diphenyl-2H-tetrazolium bromide (MTT), indocyanine green (ICG), bovine serum albumin (BSA) and enzymes were obtained from Sigma-Aldrich. Anti-LAP antibody was purchased from proteintech, USA. HepG2 cells and fetal bovine serum (FBS) were purchased from KeyGEN BioTECH Co., Ltd. (Nanjing, China). Reactive oxygen species (ROS) were prepared by the previously reported method.[1] Ultrapure water (over 18 MΩ·cm) from a Milli-Q reference system (Millipore) was used throughout. The stock solutions of the synthesized NIR-II-F1 ~ NIR-II-F4 or probes (NIR-II-F2LAP and NIR-II-F3LAP) were prepared in water or DMSO.

Apparatus. ^{1}H and ^{13}C NMR spectra were acquired by Bruker Avance III HD 400. High-resolution electrospray ionization mass spectra (HR-ESI-MS) were recorded on APEX IV FTMS (Bruker, Daltonics), and ESI-MS on Shimadzu LCMS 2020. High-performance liquid chromatography (HPLC) analyses were made with LC-20AD solvent delivery unit, SPD-M20A diode array detector (Shimadzu), and Shim-pack GIST-HP C18 column. UV-vis absorption spectra were conducted on Lambda 1050+ UV/VIS/NIR spectrophotometer (PerkinElmer). Fluorescence spectra were measured on NIR Quest-512 spectrophotometer (Ocean Optics) in 1×1 cm quartz cell, with 808 nm laser excitation. *In vivo* fluorescence imaging was performed on *In vivo* NIR-II imaging system (*In Vivo* Master, Wuhan Grand-imaging Technology) equipped with InGaAs camera C-RED2 (Firstlight); the excitation was 808 nm laser (Wuhan Grand-imaging Technology), and the excitation intensity was about 100 mW/cm^2. The exposure time (ET) of images was indicated in the corresponding figures. The emission was collected with a 1000, 1150 or 1300 nm long-pass (LP) emission filter (Edmund Optics).

Fluorescence quantum yield (Φ) determination. Φ was measured following the previous method[2] with IR26 (Φ = 0.05% in dichloroethane) as the reference.[3] The excitation wavelength was at 808 nm while keeping the absorbance below 0.05.

General procedure for LAP detection. LAP was dissolved in H_2O to provide the stock solution (10 U/mL). Unless otherwise stated, all the measurements were made in pH 7.4 phosphate buffered saline (PBS). A 5-mL of the mixture solution containing probe

(final concentration, 10 μM), an appropriate volume of PBS and LAP (10 U/mL) reacted at 37 °C for 30 min. Then 3 mL of the reaction solution was transferred to a quartz cell to measure the absorbance against the corresponding reagent blank or fluorescence spectra with 808 nm laser excitation.

Cytotoxicity assay. HepG2 cells were cultured in DMEM supplemented with 10% (v/v) FBS and 1% (v/v) penicillin-streptomycin at 37 °C in a humidified 5% CO_2 incubator. Cytotoxicity of NIR-II-F2 and NIR-II-F2LAP to HepG2 cells was investigated by standard MTT assays.[4]

***In vivo* imaging of mice.** Seven-week-old female BALB/c nude mice were purchased from Beijing Vital River Laboratory Animal Technology Co., Ltd. All animal experimental procedures were performed in accordance with the Guide for the Care and Use of Laboratory Animals, and were approved (approval number: SYXK 2017-0033) by Beijing Vital River Laboratory Animal Technology Co., Ltd. For the *in vivo* fluorescence imaging, NIR-II-F2 (200 μL, 500 μM in saline with 2% DMSO) was intravenously injected into the mouse.

Drug-induced hepatotoxicity imaging. Acetaminophen (APAP) was dissolved in warm saline (15 mg/mL). Six-week-old female BALB/c mice were given oral gavage of saline or APAP (300 mg kg^{-1}), respectively. After 12 h, the mice were intravenously injected by NIR-II-F2LAP (200 μL, 500 μM in saline with 2% DMSO), followed by the *in vivo* NIR-II imaging with 1000 nm LP filter (the hair of mice was shaved before imaging). For the imaging of dissected organs, 1000 nm LP filter was used.

2. Syntheses and characterization

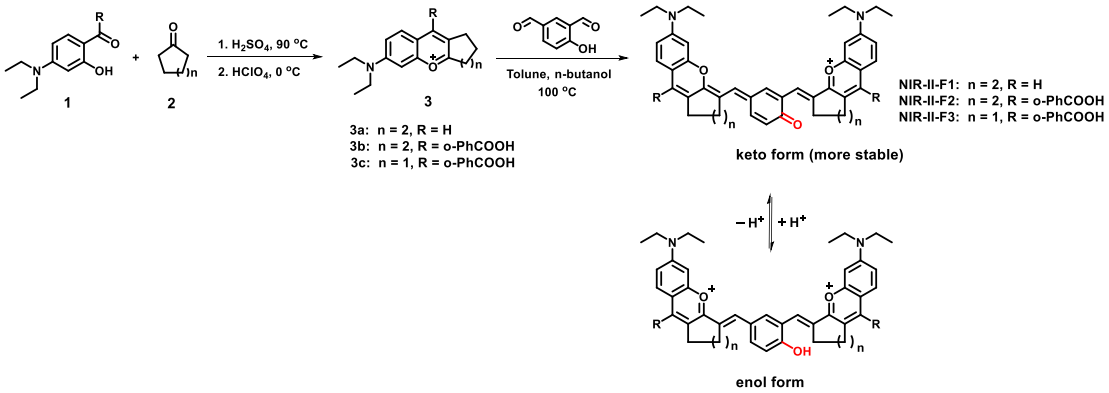

Scheme S1. Syntheses of NIR-II-F1 ~ NIR-II-F3.

Compound 3: 10 mmol of cyclohexanone or cyclopentanone was added dropwise to concentrated H_2SO_4 (10 mL) at 0 °C. After stirring for 15 min, compound **1** (5 mmol)

was added with vigorous stirring. The mixture was heated at 90 °C for 2 h, cooled down to room temperature, and poured onto crushed ice (100 g). Then perchloric acid (70%; 2 mL) was added dropwise to the mixture, and stirred for 15 min. The precipitate was filtered off and washed with cold water (200 mL). Compound **3** was obtained as a red solid and used for the next step without further purification.

NIR-II-F1 ~ NIR-II-F3: Compound **3** (0.2 mmol) and 4-hydroxyisophthalaldehyde (0.1 mmol, 15 mg) were added to the solution of toluene (5 mL) and *n*-butanol (5 mL). The reaction mixture was heated at 100 ºC for 12 h. The solvent was then removed under reduced pressure. The residues were purified by silica gel chromatography with CH_2Cl_2/MeOH (30:1 to 10:1, v/v) as the eluent to obtain **NIR-II-F1 ~ NIR-II-F3**.

NIR-II-F1 was obtained in 51% yield. ^{1}H NMR (400 MHz, MeOD; Figure S1) δ 8.35 (s, 1H), 8.11 (s, 1H), 7.84 (d, *J* = 9.6 Hz, 1H), 7.57 (d, *J* = 2.4 Hz, 1H), 7.50 (dd, *J* = 8.8, 3.0 Hz, 1H), 7.42 (dd, *J* = 9.2, 2.4 Hz, 1H), 7.21 (d, *J* = 2.4 Hz, 1H), 7.02 (d, *J* = 8.4 Hz, 1H), 6.93 (d, *J* = 8.8 Hz, 1H), 6.76 (s, 1H), 6.60 (s, 1H), 6.36 (dd, *J* = 8.8, 2.8 Hz, 1H), 6.07 (d, *J* = 2.4 Hz, 1H), 3.76 (q, *J* = 7.2 Hz, 4H), 3.20-3.30 (m, 4H), 3.02-3.10 (m, 2H), 2.92-2.97 (m, 2H), 2.35-2.60 (m, 4H), 1.95-2.02 (m, 2H), 1.75-1.90 (m, 2H), 1.35 (t, *J* = 7.2 Hz, 6H), 1.08 (t, *J* = 7.2 Hz, 6H). ^{13}C NMR (100 MHz, MeOD; Figure S2) δ 164.92, 160.60, 157.83, 153.67, 152.85, 150.23, 149.64, 138.43, 135.56, 133.15, 133.11, 130.86, 130.76, 130.41, 128.17, 128.02, 127.06, 124.81, 124.06, 123.61, 122.33, 120.62, 119.39, 118.29, 107.31, 100.39, 98.47, 96.67, 47.19, 45.43, 33.08, 30.76, 28.46, 23.74, 22.71, 21.99, 14.44, 12.88. HR-ESI-MS: *m/z* calcd for $C_{42}H_{45}N_2O_3$ $[M]^+$, 625.3425; found, 625.3421.

NIR-II-F2 was obtained in 45% yield. ^{1}H NMR (400 MHz, MeOD; Figure S3) δ 8.30 (d, *J* = 1.6 Hz, 2H), 8.28 (s, 1H), 8.21 (s, 1H), 7.70-7.85 (m, 5H), 7.67 (dd, *J* = 8.8, 1.6 Hz, 1H), 7.32 (t, *J* = 7.6 Hz, 2H), 7.17-7.28 (m, 4H), 7.06-7.17 (m, 3H), 3.65-3.78 (m, 8H), 2.95-3.10 (m, 4H), 2.40-2.50 (m, 4H), 1.80-1.95 (m, 4H), 1.32 (m, 12H). ^{13}C NMR (100 MHz, MeOD; Figure S4) δ 169.68, 164.91, 164.83, 164.78, 163.68, 162.68, 160.13, 159.99, 159.88, 157.34, 157.08, 138.35, 136.17, 136.09, 135.55, 135.37, 133.84, 132.79, 132.63, 132.37, 132.32, 131.34, 131.27, 131.20, 131.10, 130.70, 130.68, 130.01, 129.89, 128.66, 127.90, 124.68, 123.95, 123.75, 119.11, 119.06, 118.71, 118.67, 117.16, 96.90, 96.52, 47.08, 47.01, 28.39, 27.18, 27.01, 22.77, 22.57, 12.95, 12.90. HR-ESI-MS: *m/z* calcd for $C_{56}H_{53}N_2O_7$ $[M]^+$, 865.3847; found, 865.3849. m.p. > 250 ºC.

NIR-II-F3 was obtained in 41% yield. ^{1}H NMR (400 MHz, DMSO-d_6; Figure S5) δ

7.91-7.98 (m, 2H), 7.74-7.82 (m, 2H), 7.64-7.72 (m, 2H), 7.50 (s, 1H), 7.32 (d, J = 8.0 Hz, 1H), 7.29 (d, J = 8.0 Hz, 2H), 7.11 (s, 1H), 6.95 (d, J = 8.4 Hz, 1H), 6.78 (s, 1H), 6.45-6.55 (m, 6H), 3.34-3.42 (m, 8H), 2.85-3.05 (m, 4H), 2.25-2.35 (m, 2H), 1.87-1.97 (m, 2H), 1.05-1.15 (m, 12H). HR-ESI-MS: *m/z* calcd for $C_{54}H_{49}N_2O_7$ $[M]^+$, 837.3534; found, 837.3538. m.p. > 250 ºC.

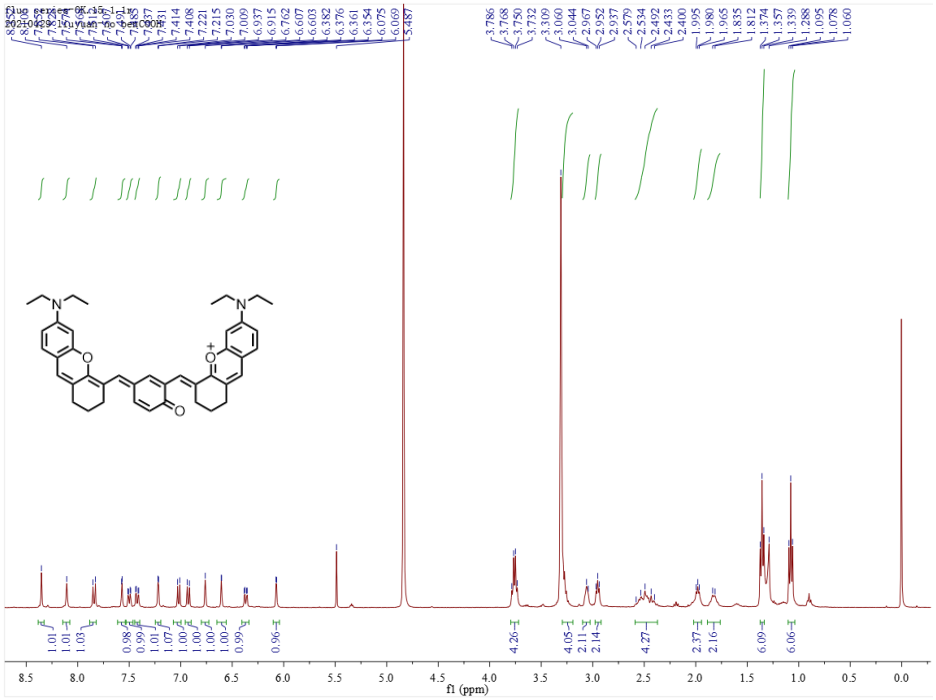

Figure S1. ^{1}H NMR spectrum of **NIR-II-F1** (400 MHz, MeOD, 298 K).

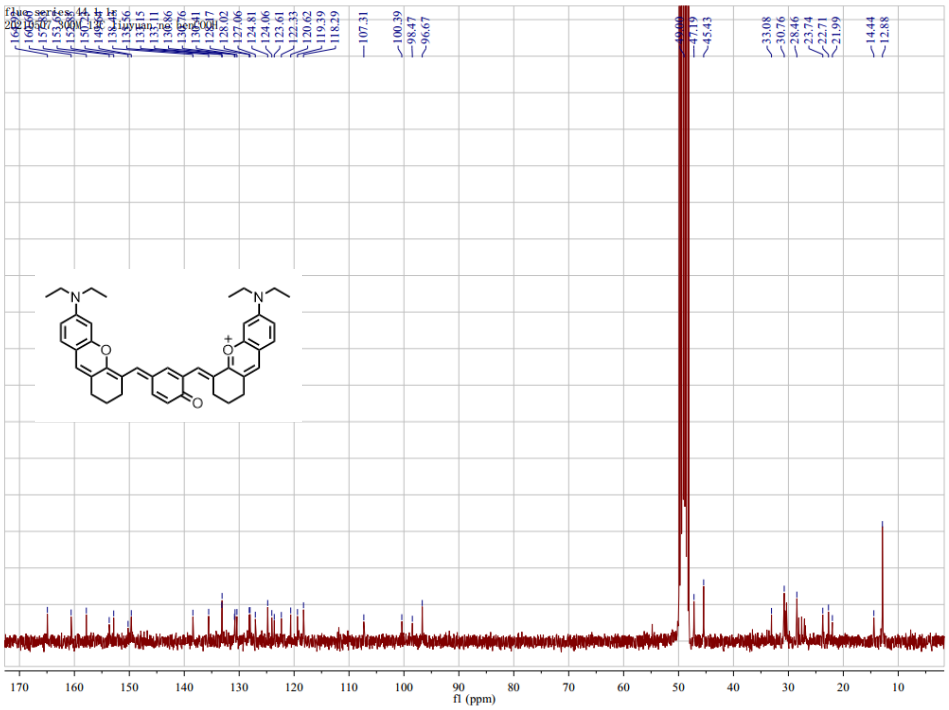

Figure S2. ^{13}C NMR spectrum of **NIR-II-F1** (100 MHz, MeOD, 298 K).

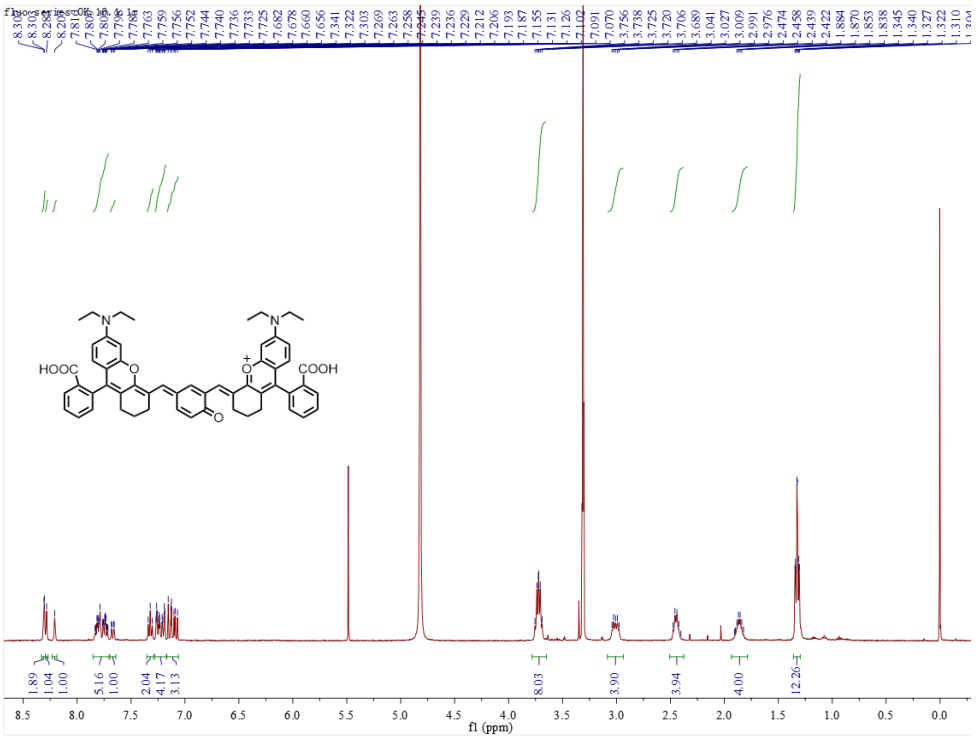

Figure S3. ^{1}H NMR spectrum of **NIR-II-F2** (400 MHz, MeOD, 298 K).

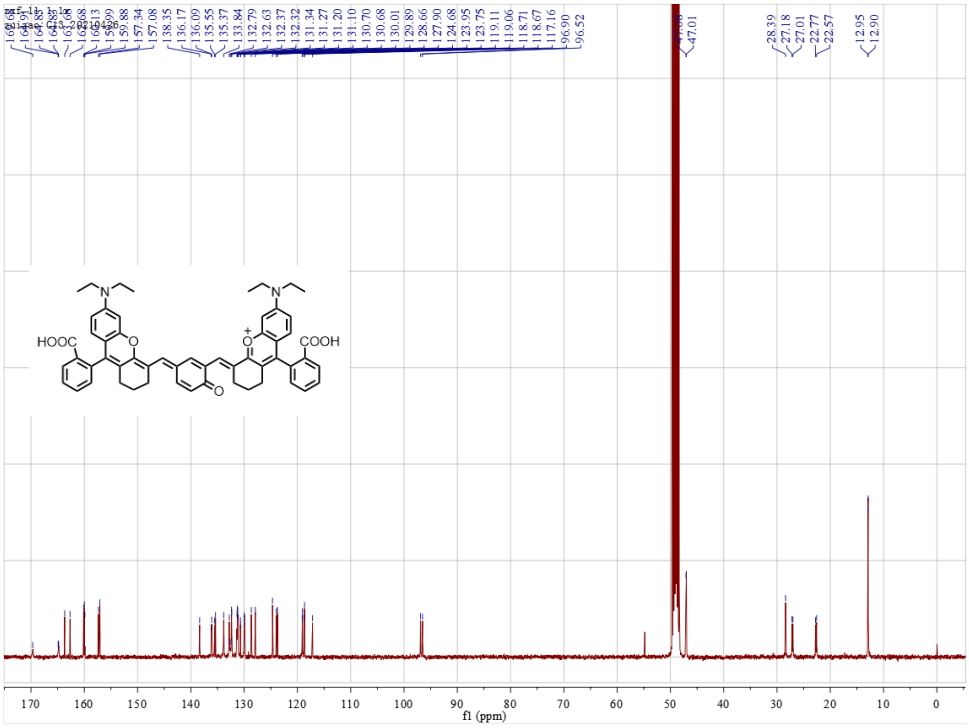

Figure S4. ^{13}C NMR spectrum of **NIR-II-F2** (100 MHz, MeOD, 298 K).

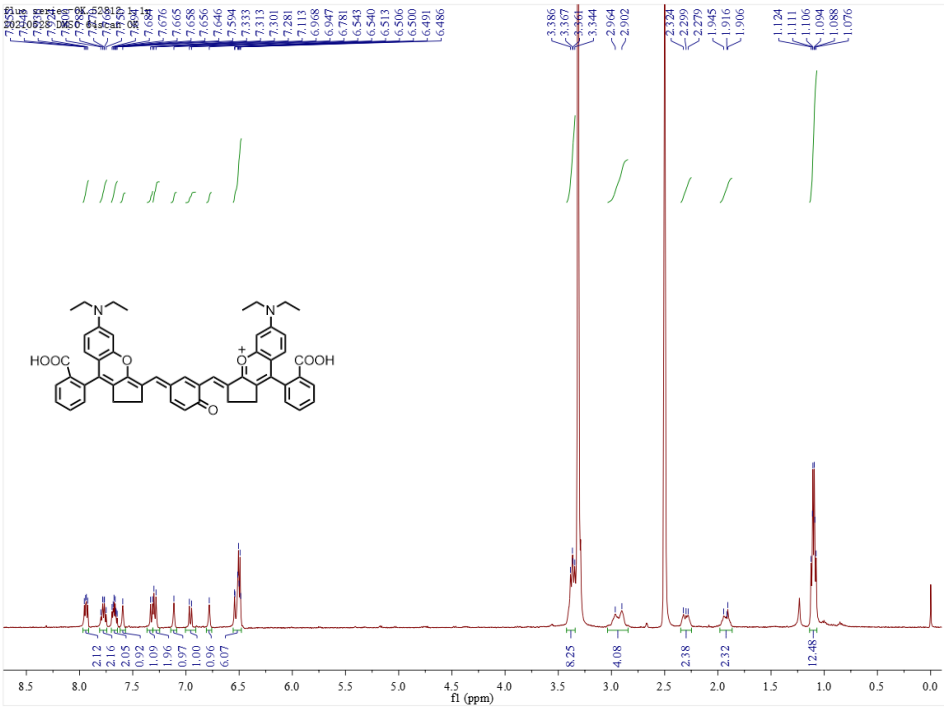

Figure S5. ^{1}H NMR spectrum of **NIR-II-F3** (400 MHz, DMSO-d$_6$, 298 K).

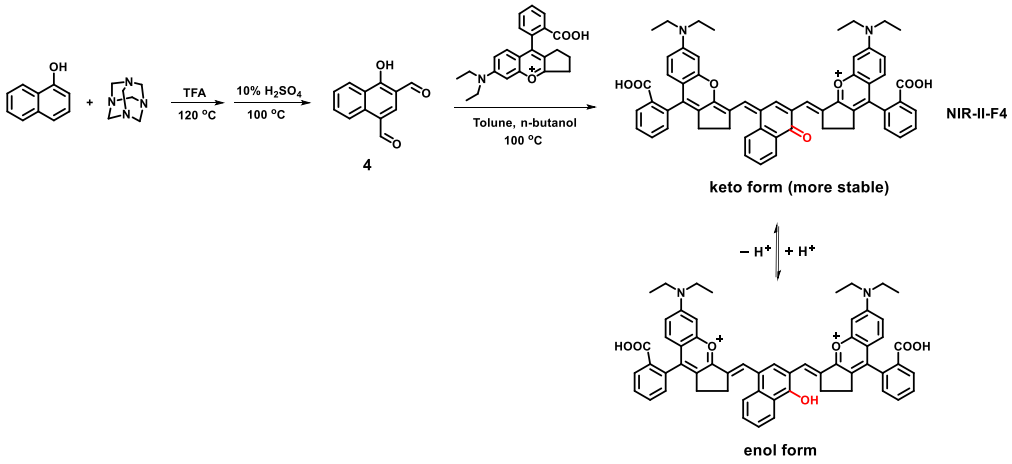

Scheme S2. Synthesis of NIR-II-F4.

NIR-II-F4: First, compound **4** was prepared following the known method.[5] In brief, 1-naphthol (10 mmol, 1.44 g) and hexamethylenetetramine (20 mmol, 2.80 g) were dissolved in trifluoroacetic acid (TFA, 10 mL), and the mixture was heated at 120 ºC for 4 h. After cooled to room temperature, 10% H_2SO_4 (5 mL) was added to the mixture, and then heated at 100 ºC for 2 h. After cooled to room temperature, the precipitate was filtered off and washed with water. The residue was purified by silica gel chromatography with CH_2Cl_2/petroleum ether (2:1, v/v) as the eluent to obtain compound **4** (30% yield). ^{1}H NMR (400 MHz, $CDCl_3$; Figure S6) δ 13.25 (s, 1H), 10.23 (s, 1H), 10.06 (s, 1H), 9.31 (d, J = 8.4 Hz, 1H), 8.53 (d, J = 8.4 Hz, 1H), 8.07 (s, 1H),

7.87 (m, 1H), 7.68 (m, 1H). m.p. 144-145 ºC. **NIR-II-F4** was then synthesized in the same way as **NIR-II-F1** ~ **NIR-II-F3** (35% yield). ^{1}H NMR (400 MHz, DMSO-d_6; Figure S7) δ 8.24-8.44 (m, 5H), 8.12-8.22 (m, 2H), 7.85 (q, J = 8.0 Hz, 2H), 7.65-7.78 (m, 3H), 7.44-7.54 (m, 3H), 6.80-7.10 (m, 6H), 3.40-3.60 (m, 8H), 3.15-3.25 (m, 4H), 2.55-2.70 (m, 4H), 1.13-1.20 (m, 12H). HR-ESI-MS: *m/z* calcd for $C_{58}H_{49}N_2O_7$ [M-2H]$^-$, 885.3534; found, 885.3547. m.p. > 250 ºC.

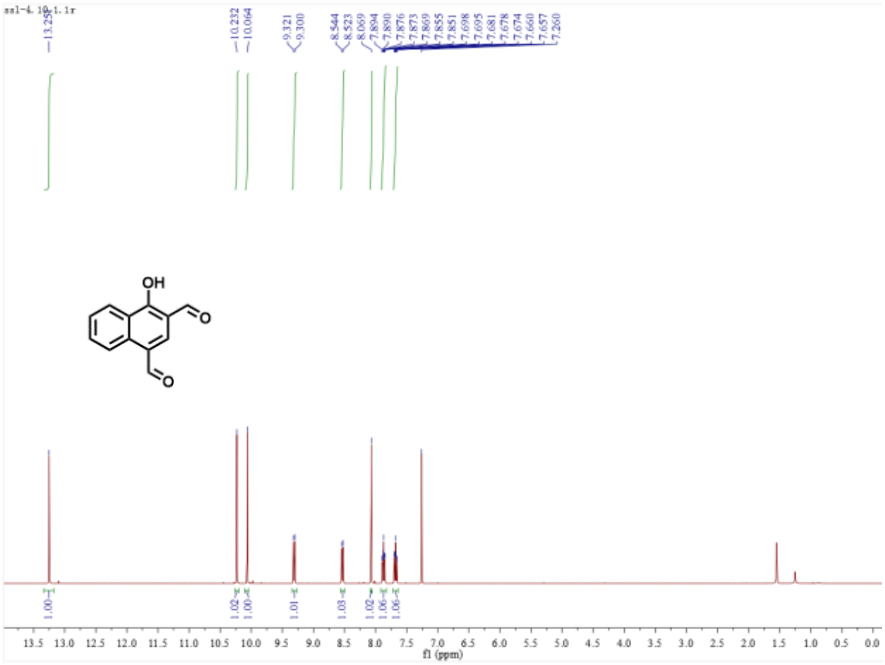

Figure S6. ^{1}H NMR spectrum of compound **4** (400 MHz, $CDCl_3$, 298 K).

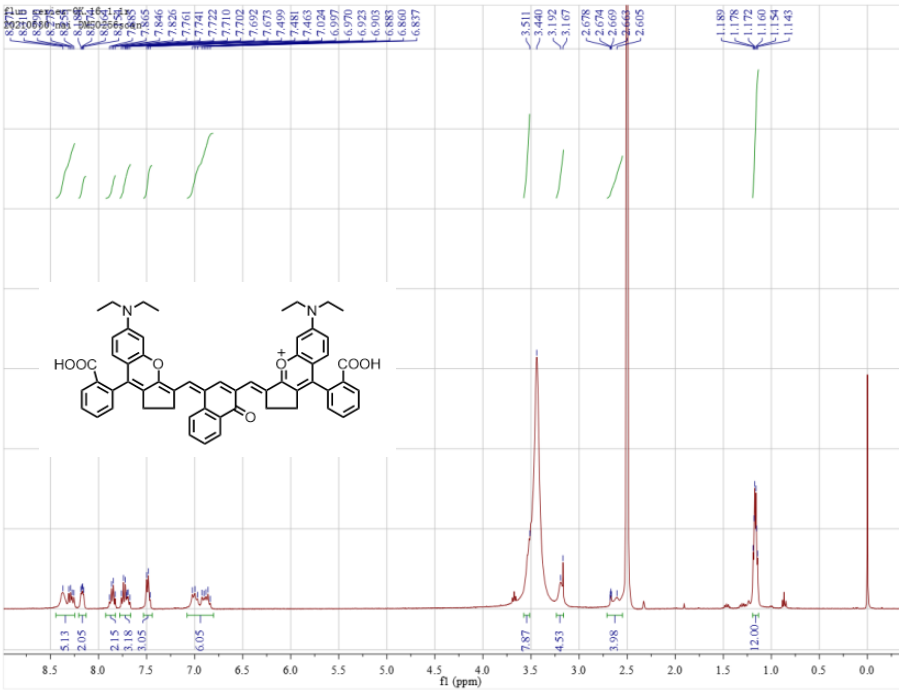

Figure S7. ^{1}H NMR spectrum of **NIR-II-F4** (400 MHz, DMSO-d_6, 298 K).

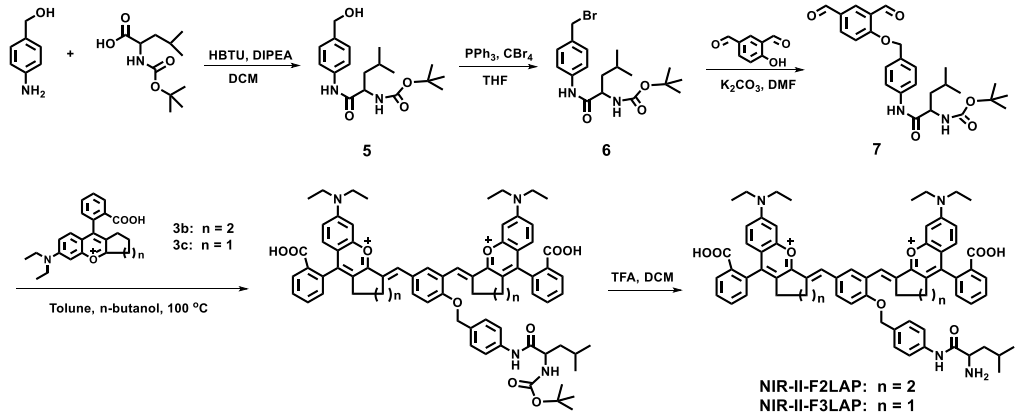

Scheme S3. Syntheses of probes NIR-II-F2LAP and NIR-II-F3LAP.

Compound 5: Boc-L-Leucine (10 mmol, 2.31 g) was dissolved in CH_2Cl_2 (100 mL), following by the addition of DIPEA (2.58 g, 20 mmol) and HBTU (12 mmol, 4.55 g). After stirring for 30 min, 4-aminobenzyl alcohol (2.46 g, 20 mmol) was added, and the mixture was stirred overnight at room temperature. Then, the mixture was diluted with water, and extracted with CH_2Cl_2. The organic layer was dried over anhydrous Na_2SO_4. The solvent was removed under reduced pressure, and the crude product was purified by silica gel chromatography with petroleum ether/ethyl acetate (2:1, v/v) as eluent to afford compound **5** (55% yield), which was then used in the next step.

Compound 6: Compound **5** (4 mmol, 1.34 g) was dissolved in dry THF (30 mL), and the mixture was cooled to 0 ºC for 5 min. CBr_4 (1.99 g, 6 mmol) and PPh_3 (1.57 g, 6 mmol) were added to the mixture while keeping at 0 ºC for 10 min. Then the resulting mixture was stirred at room temperature for 2 h. The solvent was then evaporated under reduced pressure. The mixture was diluted with water, and extracted with CH_2Cl_2. Then, the organic layer was dried over anhydrous Na_2SO_4. The solvent was removed by evaporation, and crude product was purified by silica gel chromatography with petroleum ether/ethyl acetate (10:1, v/v) as the eluent to afford compound **6** (59% yield).

Compound 7: Compound **6** (2 mmol, 0.80 g), 4-hydroxyisophthalaldehyde (2 mmol, 0.30 g) and potassium carbonate (4.0 mmol, 0.55 g) were added to dry DMF (20 mL) and stirred overnight at room temperature. Then the mixture was diluted with water, and extracted with CH_2Cl_2. Next, the organic layer was dried over anhydrous Na_2SO_4. The solvent was then evaporated under reduced pressure, and the crude product was purified by silica gel chromatography with petroleum ether/ethyl acetate (4:1, v/v) as eluent to afford compound **7** (70% yield). ^{1}H NMR (400 MHz, $CDCl_3$; Figure S8) δ 10.50 (s, 1H), 9.94 (s, 1H), 8.59 (br, 1H), 8.33 (d, J = 2.4 Hz, 1H), 8.09 (dd, J = 8.8, 2.4 Hz, 1H), 7.57 (d, J = 8.4 Hz, 2H), 7.36 (d, J = 2.4 Hz, 2H), 7.18 (d, J = 8.8 Hz, 1H),

5.23 (s, 2H), 4.98 (d, J = 8.0 Hz, 1H), 4.25 (br, 1H), 1.70-1.80 (m, 2H), 1.52-1.62 (m, 1H), 1.45 (s, 9H), 0.97 (t, J = 6.8 Hz, 6H). ^{13}C NMR (100 MHz, $CDCl_3$; Figure S9) δ 190.28, 188.61, 171.79, 165.00, 156.65, 138.67, 135.83, 131.75, 130.34, 129.75, 128.38, 124.99, 120.13, 113.65, 70.90, 54.00, 41.03, 28.43, 24.84, 23.15, 21.82. HR-ESI-MS: *m/z* calcd for $C_{26}H_{32}N_2NaO_6$ $[M+Na]^+$, 491.2158; found, 491.2153. m.p. 83-84 ºC.

NIR-II-F2LAP or **NIR-II-F3LAP:** Compound **7** (0.1 mmol, 47 mg) and **3b** or **3c** (0.2 mmol) were added to the solution of toluene (5 mL) and *n*-butanol (5 mL). The reaction mixture was heated at 100 ºC for 12 h. The solvent was removed by evaporation. Next, 3 mL CH_2Cl_2 was added to the residue, and a solution of TFA (1.5 mL) in CH_2Cl_2 (1.5 mL) was added dropwise to the mixture at 0 ºC. Then the mixture was stirred at room temperature for 5 min. The solvent was removed by evaporation, and the residue was purified by silica gel chromatography with CH_2Cl_2/MeOH (30:1 to 10:1, v/v) as the eluent to obtain **NIR-II-F2LAP** or **NIR-II-F3LAP**.

NIR-II-F2LAP was obtained in 28% yield. ^{1}H NMR (400 MHz, MeOD; Figure S10) δ 8.32 (t, J = 4.8 Hz, 3H), 8.23 (s, 1H), 7.74-7.89 (m, 6H), 7.62-7.72 (m, 2H), 7.51-7.60 (m, 2H), 7.23-7.43 (m, 6H), 7.10-7.20 (m, 3H), 5.30-5.52 (m, 2H), 4.06 (t, J = 7.2 Hz, 1H), 3.70-3.80 (m, 8H), 3.00-3.10 (m, 2H), 2.90-3.00 (m, 2H), 2.40-2.50 (m, 4H), 1.70-2.00 (m, 7H), 1.30-1.40 (m, 12H), 1.02-1.08 (m, 6H). ^{13}C NMR (100 MHz, MeOD; Figure S11) δ 169.13, 168.31, 168.25, 165.39, 164.90, 163.32, 162.48, 160.32, 160.20, 159.93, 157.66, 157.41, 139.15, 137.32, 136.16, 136.11, 135.31, 134.43, 134.38, 134.28, 132.63, 131.49, 131.43, 131.34, 131.27, 131.16, 131.05, 131.00, 130.11, 129.98, 129.79, 129.47, 129.45, 129.05, 126.63, 124.04, 123.94, 123.87, 121.34, 119.56, 119.46, 119.17, 119.02, 114.32, 114.26, 96.61, 96.36, 53.74, 47.23, 47.05, 41.76, 28.23, 27.12, 26.97, 25.50, 23.21, 22.75, 22.60, 22.03, 12.87, 12.80. HR-ESI-MS: *m/z* calcd for $C_{69}H_{72}N_4O_8$ $[M]^{2+}$, 542.2670; found, 542.2667.

NIR-II-F3LAP was obtained in 30% yield. ^{1}H NMR (400 MHz, MeOD; Figure S12) δ 8.30 (d, J = 8.0 Hz, 2H), 8.15 (s, 1H), 8.03 (s, 1H), 7.64-7.87 (m, 8H), 7.48-7.56 (m, 2H), 7.36-7.44 (m, 2H), 7.14-7.34 (m, 7H), 5.42 (s, 2H), 4.00-4.10 (m, 1H), 3.60-3.80 (m, 8H), 3.15-3.30 (m, 4H), 2.75-2.90 (m, 4H), 1.70-1.90 (m, 3H), 1.25-1.34 (m, 12H), 1.01-1.05 (m, 6H). HR-ESI-MS: *m/z* calcd for $C_{67}H_{68}N_4O_8$ $[M]^{2+}$, 528.2513; found, 528.2513.

It should be noted that ^{13}C NMR of all the compounds (**NIR-II-F3**, **NIR-II-F4**, **NIR-II-F3LAP**) with a five-membered ring cannot be obtained, possibly due to the complex

isomerization caused by the increased molecular planarity, which may inhibit the rotation of ortho-PhCOOH.

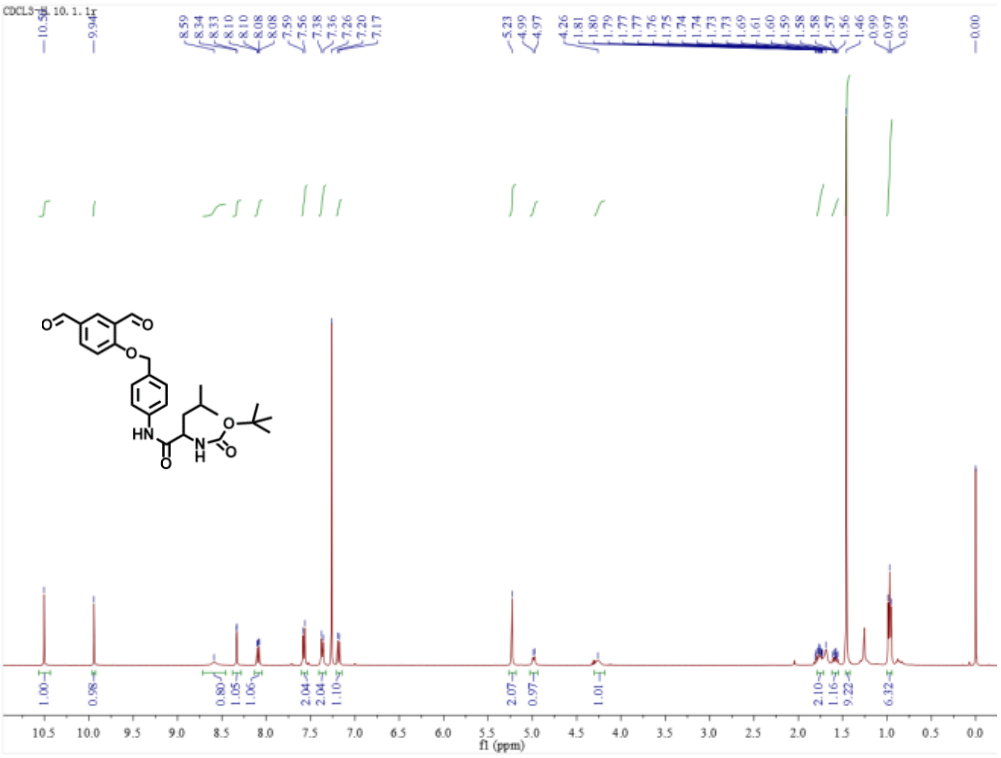

Figure S8. ^{1}H NMR spectrum of compound **7** (400 MHz, $CDCl_3$, 298 K).

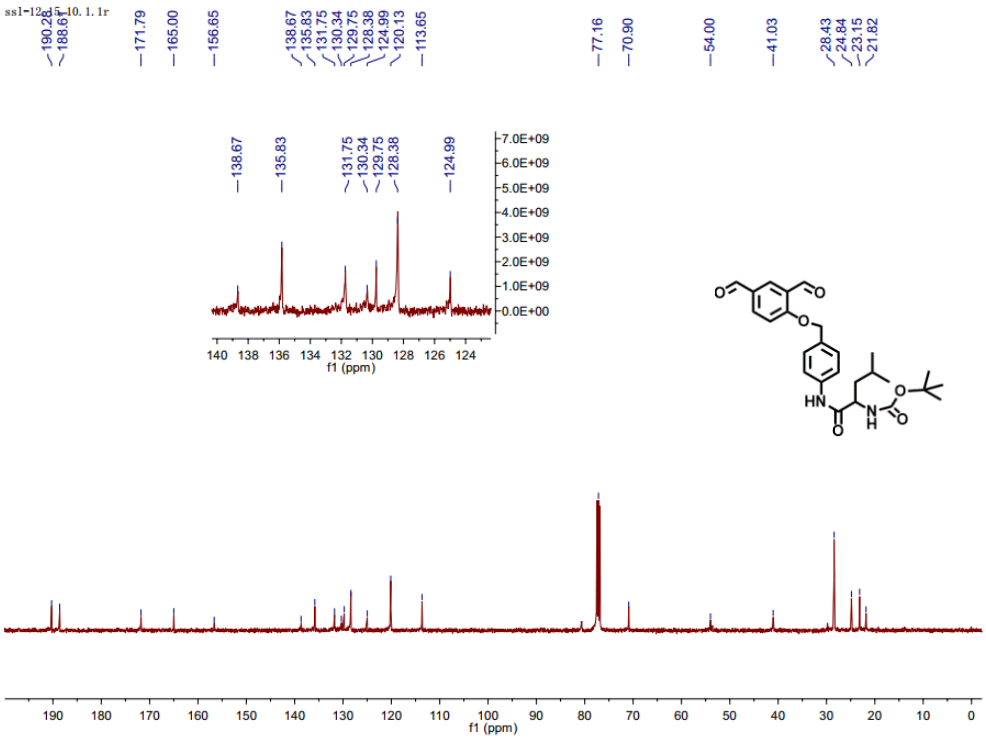

Figure S9. ^{13}C NMR spectrum of compound **7** (100 MHz, $CDCl_3$, 298 K).

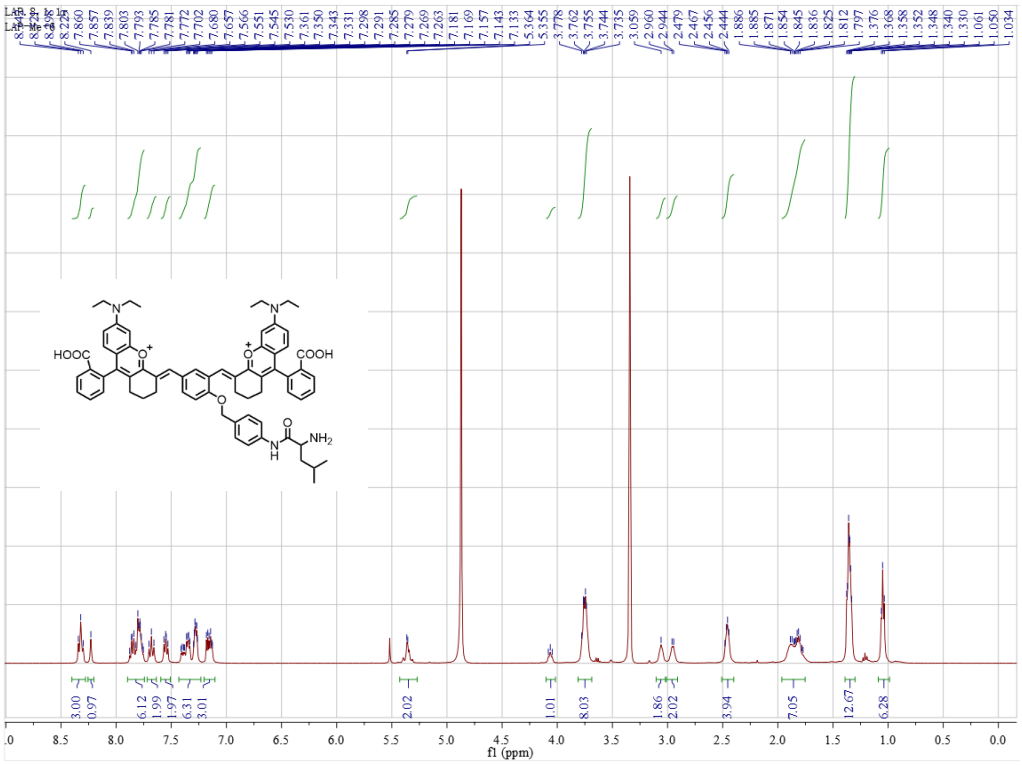

Figure S10. ^{1}H NMR spectrum of **NIR-II-F2LAP** (400 MHz, MeOD, 298 K).

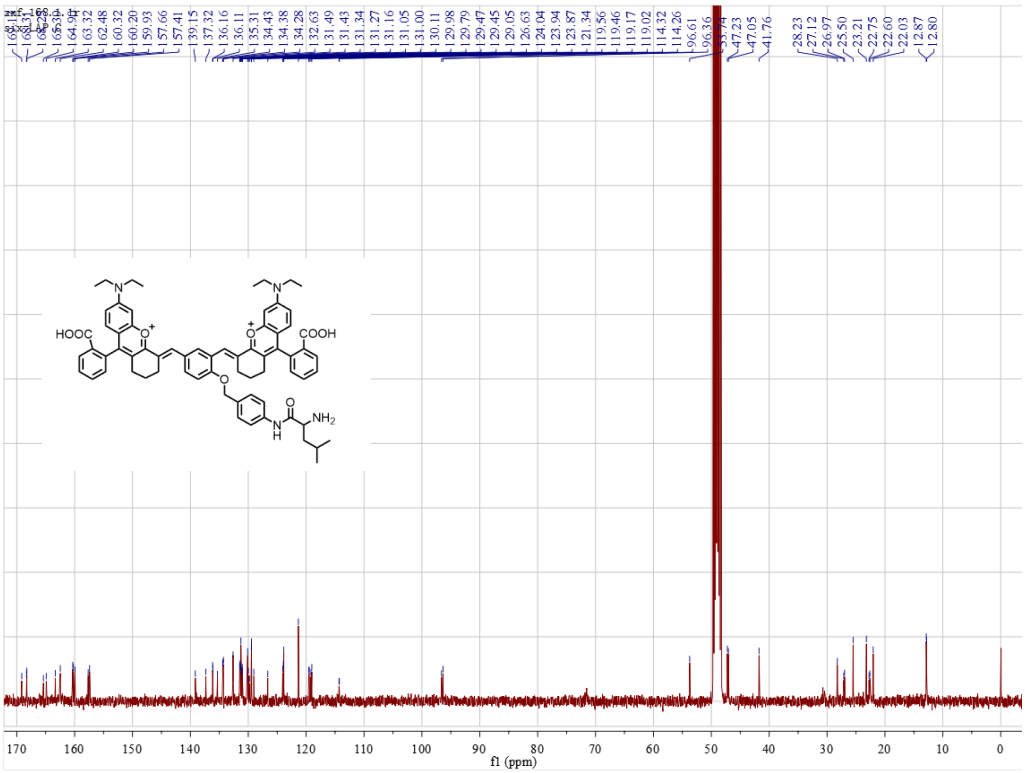

Figure S11. ^{13}C NMR spectrum of **NIR-II-F2LAP** (100 MHz, MeOD, 298 K).

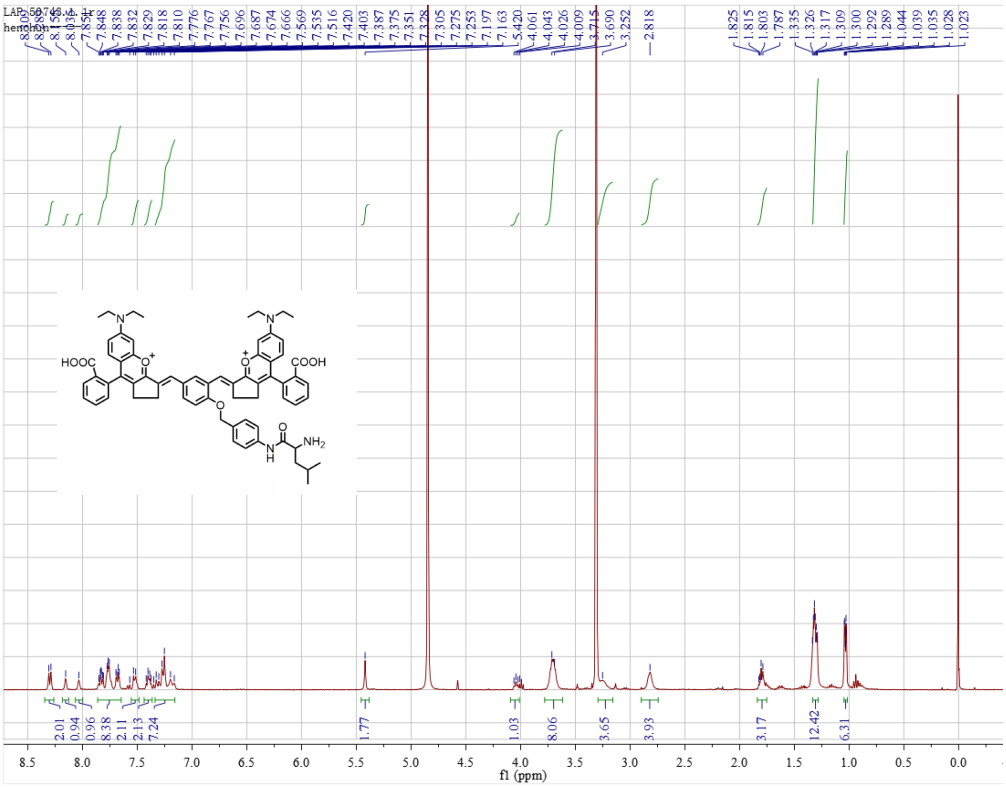

Figure S12. ^{1}H NMR spectrum of **NIR-II-F3LAP** (400 MHz, MeOD, 298 K).

3. Supplementary tables and figures

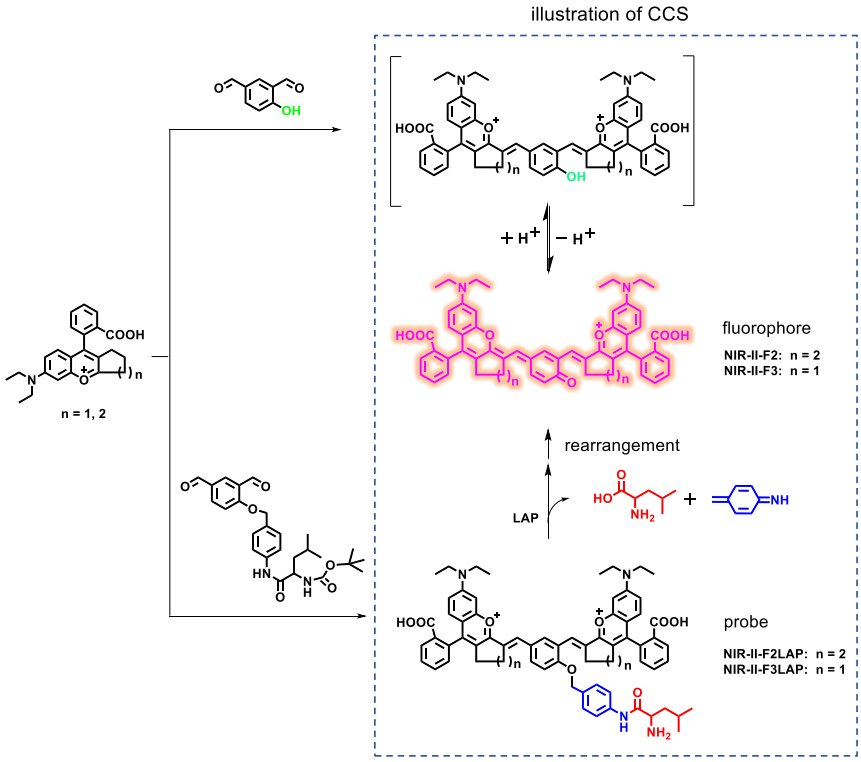

Figure S13. Design and detection mechanism of NIR-II probes with CCS feature.

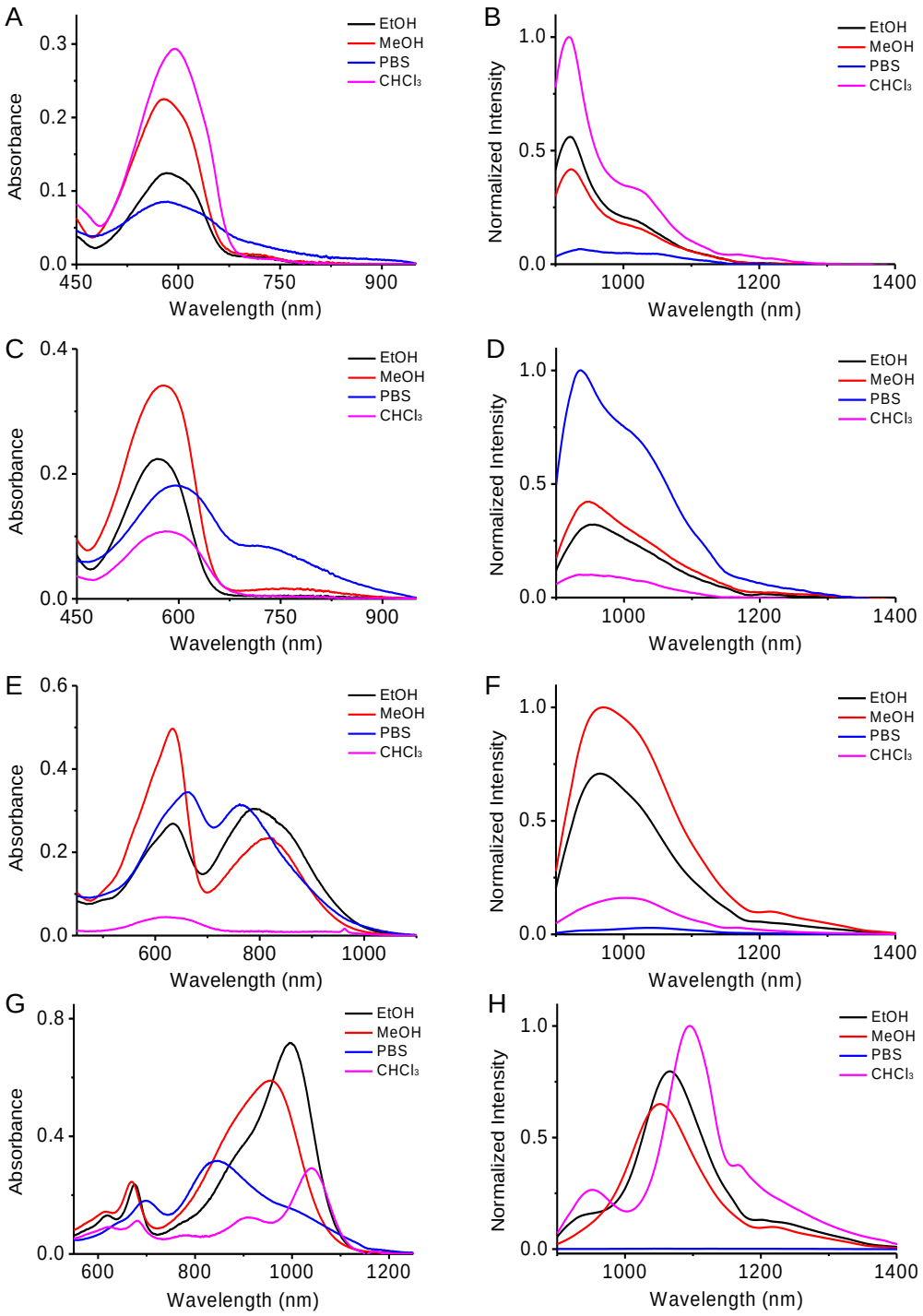

Figure S14. Absorption (A, C, E, G) and fluorescence emission (B, D, F, H) spectra of the fluorophores (10 μM) in different solvents. (A, B) NIR-II-F1; (C, D) NIR-II-F2; (E, F) NIR-II-F3; (G, H) NIR-II-F4. λ_{ex} = 808 nm.

Table S1. Photophysical data of fluorophores in pH 7.4 PBS.

fluorophores	λ_{abs} (nm)[a]	ε (10^4 $M^{-1}cm^{-1}$)[b]	λ_{em} (nm)[c]	Φ (%)[d]	brightness ($M^{-1}cm^{-1}$)
NIR-II-F1	585/740	1.3 (at 585 nm)	940 (nearly flat)	-	-
NIR-II-F2	595/740	1.9 (at 595 nm)	940	0.02	3.8
NIR-II-F3	660/760	3.8 (at 660 nm)	1040	0.004	1.5
NIR-II-F4	700/850	3.1 (at 850 nm)	1050 (nearly flat)	-	-

[a] Absorption peaks. [b] Molar absorptivity of the strongest absorption peak.
[c] Fluorescence emission peak. [d] IR26 (Φ = 0.05% in dichloroethane) was used as the reference.

Table S2. The solubility of compounds in water and DMSO at 25 °C.

compounds[a]	solubility (%, w/v)	
	water	DMSO
NIR-II-F1 (control)	＜0.01	＞0.1
NIR-II-F2	0.02	＞0.1
NIR-II-F3	＞0.03	＞0.1
NIR-II-F4	＞0.03	＞0.1
NIR-II-F2LAP	0.02	＞0.1
NIR-II-F3LAP	＞0.03	＞0.1

[a] All the compounds are soluble in water and more easily soluble in DMSO.

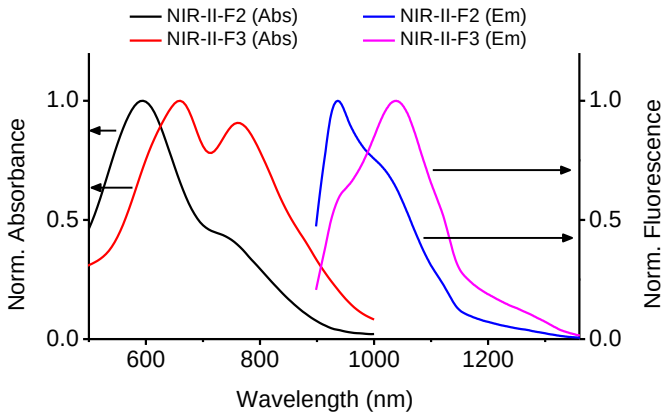

Figure S15. Normalized absorption and fluorescence spectra of 10 μM of NIR-II-F2 and NIR-II-F3 in pH 7.4 PBS.

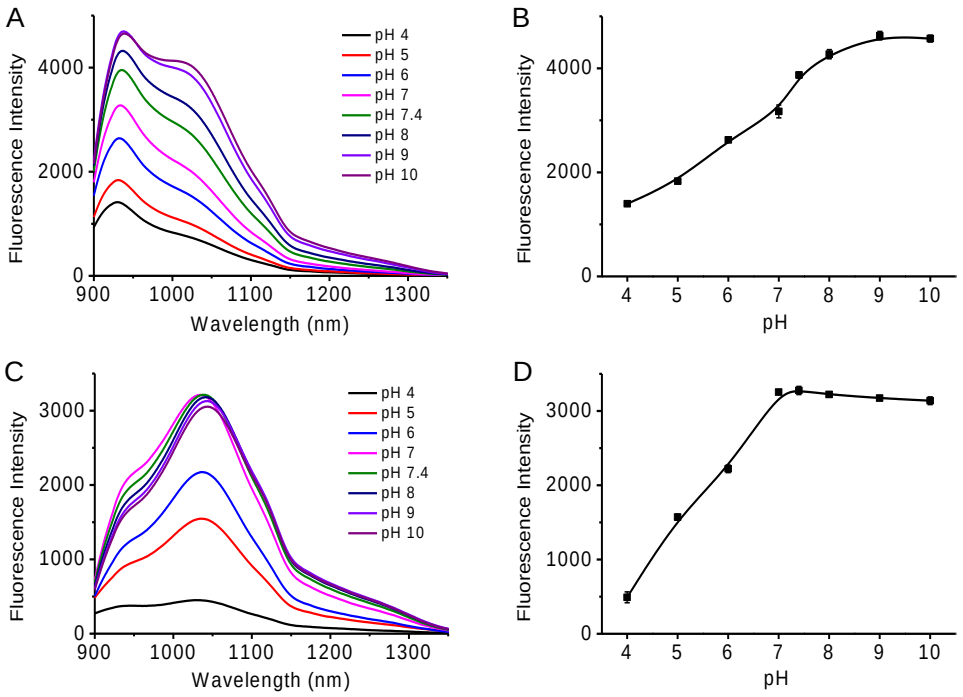

Figure S16. Effects of pH on the fluorescence of 10 μM of NIR-II-F2 (A, B) and NIR-II-F3 (C, D) in PBS with different pH values. λ_{ex} = 808 nm. The fluorescence emission of NIR-II-F2 and NIR-II-F3 was measured at 940 and 1040 nm, respectively.

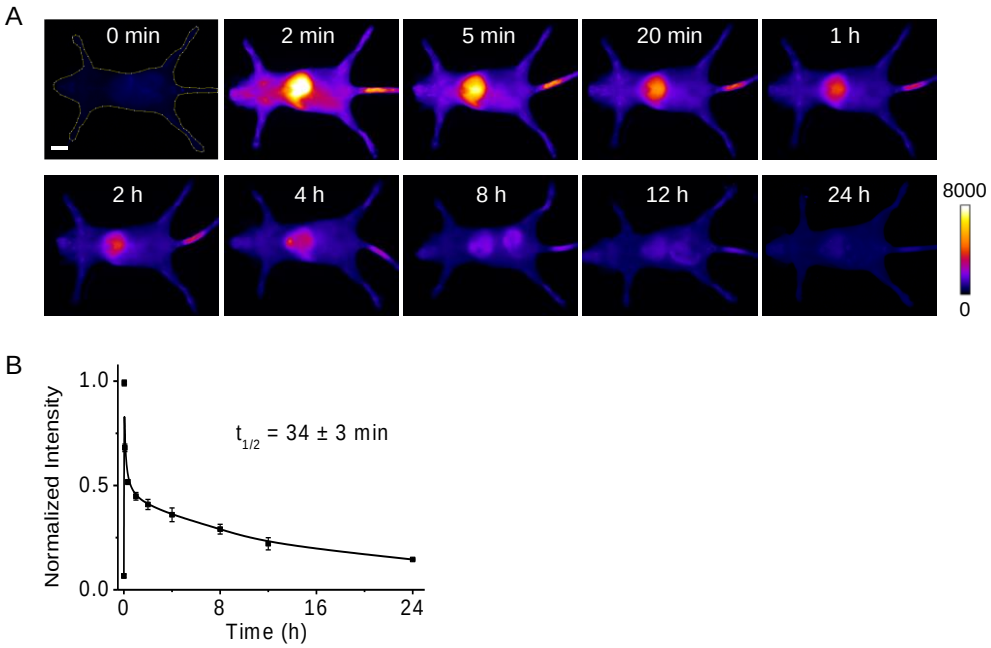

Figure S17. Fluorescence intensity kinetics of NIR-II-F2 in the blood circulation of mice. (A) Representative images at various time points (0-24 h) after intravenous injection of NIR-II-F2 (500 μM, 200 μL). Excitation: 808 nm laser. Scale bar: 1 cm. (B) Normalized fluorescence of NIR-II-F2 in mice versus time. The maximal fluorescence intensity (2 min in panel A) is defined as 1.0. Results are the mean ± SD (n = 3; there were three mice).

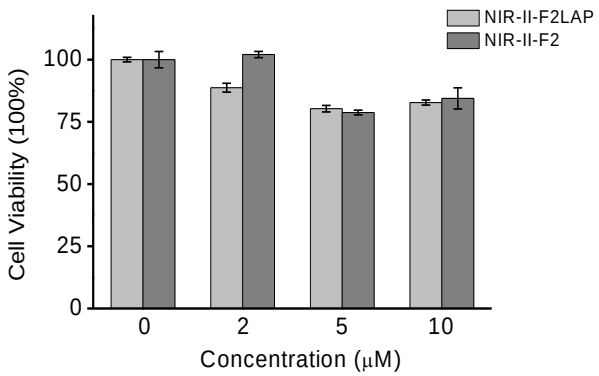

Figure S18. Cell viability of HepG2 cells treated with NIR-II-F2LAP and NIR-II-F2 for 24 h. Results are the mean ± SD (n = 5).

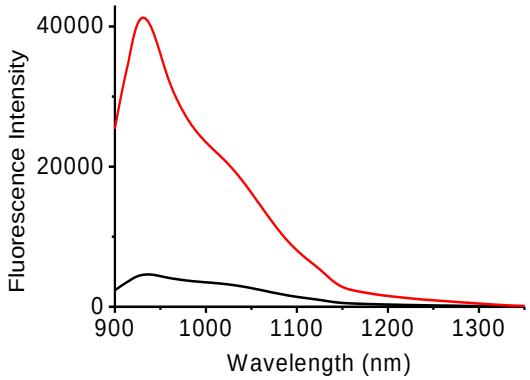

Figure S19. Fluorescence spectra of 10 μM of NIR-II-F2 in pH 7.4 PBS in the absence (black) or presence (red) of 100 μM BSA.

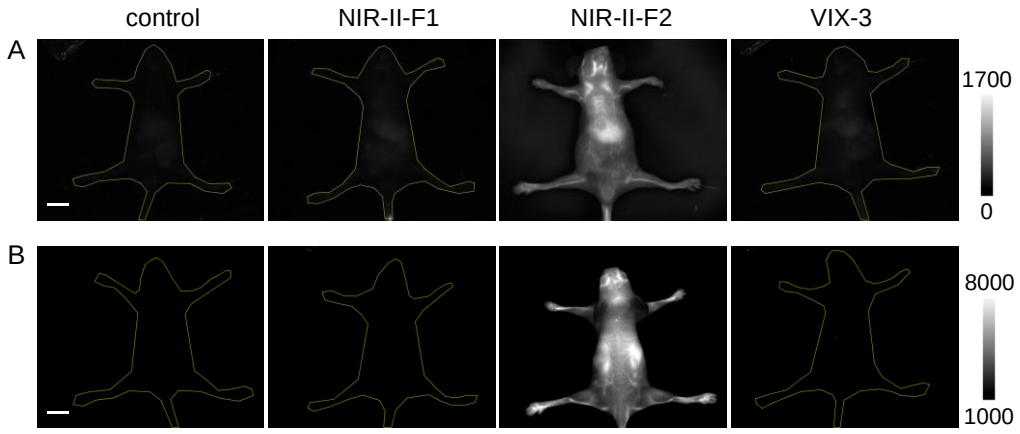

Figure S20. Fluorescence images of mice with 1150 nm LP filter after injection of 200 μL of 500 μM NIR-II-F1, NIR-II-F2 or VIX-3 from (A) ventral and (B) dorsal views. Excitation: 808 nm laser. Control: the images of mice without dye. For panel A, ET = 40 ms; for panel B, ET = 250 ms. Scale bars: 1 cm.

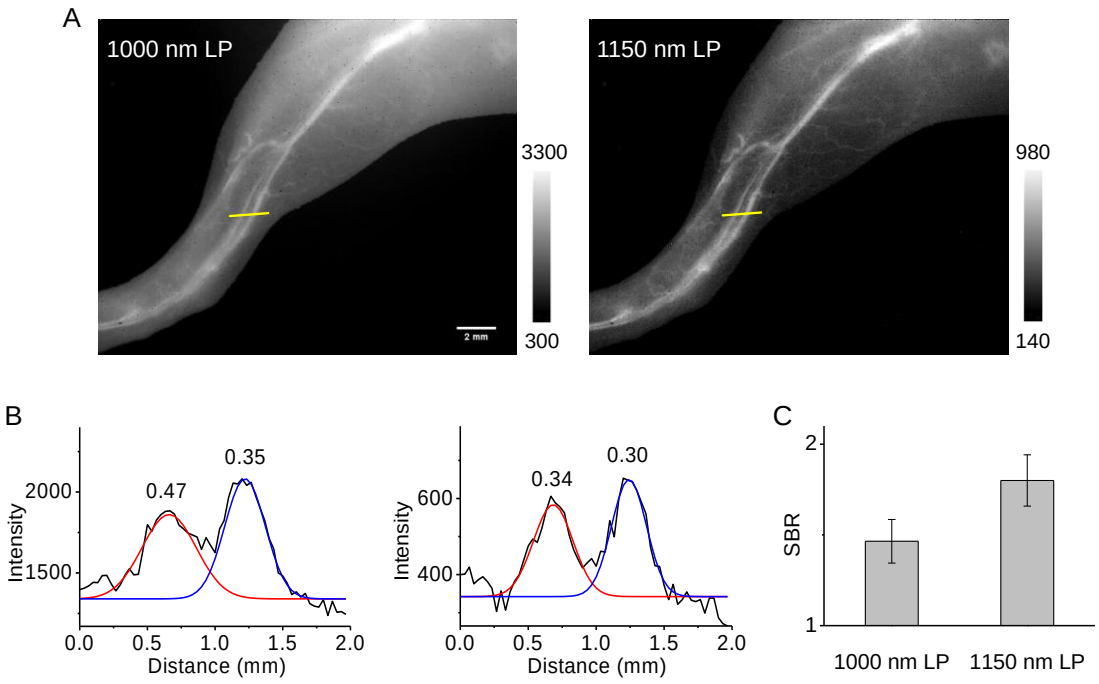

Figure S21. (A) Femoral vascular images with 1000 or 1150 nm LP filter using higher magnification lens after injection of NIR-II-F2 (500 μM, 200 μL). ET = 500 ms. Excitation: 808 nm laser. Scale bar: 2 mm. (B) Intensity profiles of the corresponding cross-sectional lines (yellow) in panel A with (left) 1000 or (right) 1150 nm LP filter. Red and blue curves are Gaussian fitting of the corresponding peaks; the full width at half-maximum (FWHM) is marked on the top of the peak. As is shown, FWHM is smaller with a longer 1150 nm LP filter. (C) Signal-background ratio (SBR) of vessels from the cross-sectional lines in panel A with 1000 or 1150 nm LP filter. SBR is obtained from the intensity ratio of vessel to adjacent tissue in the cross-sectional line.

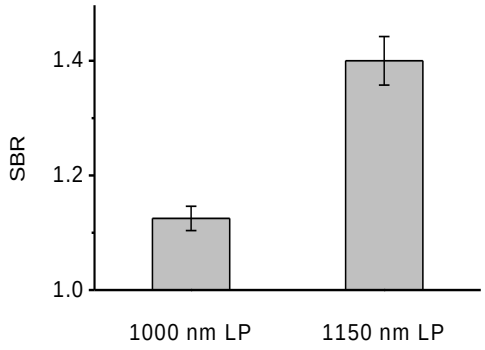

Figure S22. SBR of abdominal vessels from the cross-sectional lines in Fig. 2B (main text) with 1000 or 1150 nm LP filter. SBR is obtained from the intensity ratio of vessel to adjacent tissue in the cross-sectional line.

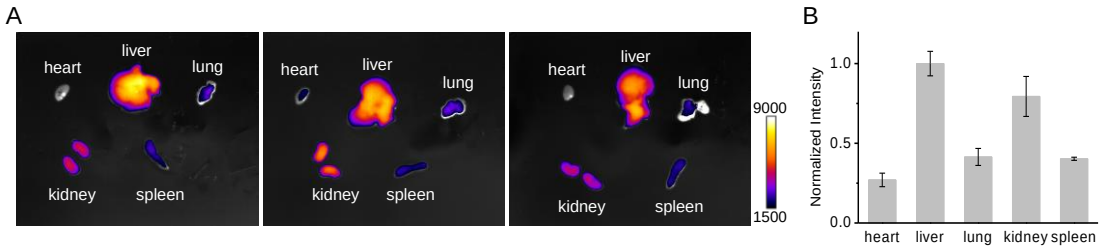

Figure S23. Ex vivo biodistribution of NIR-II-F2 in mice. (A) Fluorescence images of the dissected organs at 12 h post-injection of NIR-II-F2 (500 μM, 200 μL). Excitation: 808 nm laser. (B) Histogram analysis of the relative fluorescence intensity in the organs in panel A. Results are the mean ± SD (n = 3; there were three mice).

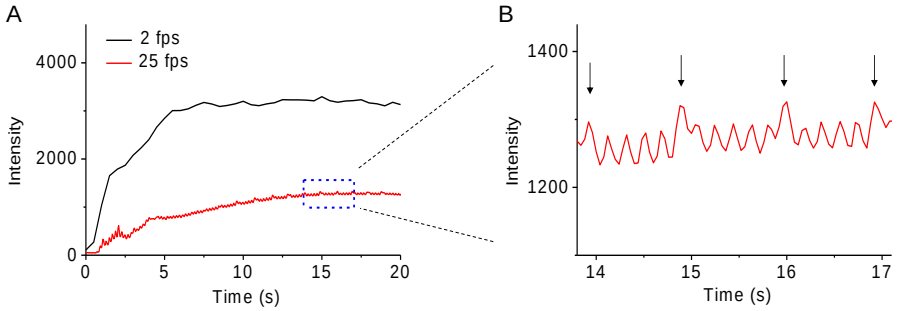

Figure S24. Heart rate measurement. (A) Fluorescence intensity changes of heart along with time in Videos S2 and S3. For Video S2: ET = 500 ms, frame rate = 2 fps, 1300 nm LP filter; for Video S3: ET = 40 ms, frame rate = 25 fps, 1150 nm LP filter. (B) Enlarged plots at 25 fps in the period of 13.8-17.1 s. Each arrow represents a respiration, which leads to the rhythmic fluctuations above the normal intensity. With Video S2, we attempted to measure the heart rate, but failed; this was due to the low frame rate of 2 fps, which inevitably resulted in the loss of data integrity. To address this issue, therefore, we conducted the imaging experiment at a higher frame rate of 25 fps (Video S3). As shown in panel B, the heart rate is determined to be 320 beats min^{-1}.

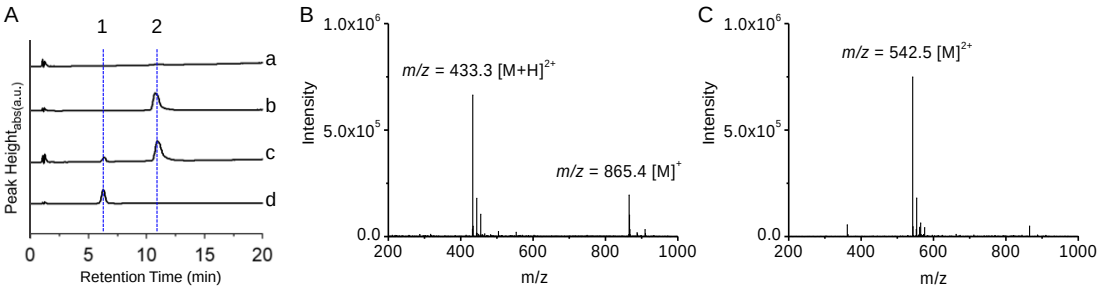

Figure S25. Reaction mechanism verification by HPLC-MS. (A) Chromatograms of different reaction systems. (a): LAP (200 U/L); (b): NIR-II-F2LAP (50 μM); (c): NIR-

II-F2LAP (50 μM) and LAP (200 U/L); (d): NIR-II-F2 (50 μM). Assignments of the peaks: (1) 6.3 min, NIR-II-F2; (2) 10.8 min, NIR-II-F2LAP. (B) ESI-MS of the separated component at peak 1 in system c of panel A. The component is ascribed to NIR-II-F2 with a mass peak at *m/z* = 865.4 $[M]^+$ and 433.3 $[M+H]^{2+}$. (C) ESI-MS of the separated component at peak 2 in system c of panel A. The component is ascribed to the remaining NIR-II-F2LAP with a mass peak at *m/z* = 542.5 $[M]^{2+}$. It can be seen that, after reaction of NIR-II-F2LAP with LAP, the chromatographic peak of the product (NIR-II-F2) appears in the reaction solution.

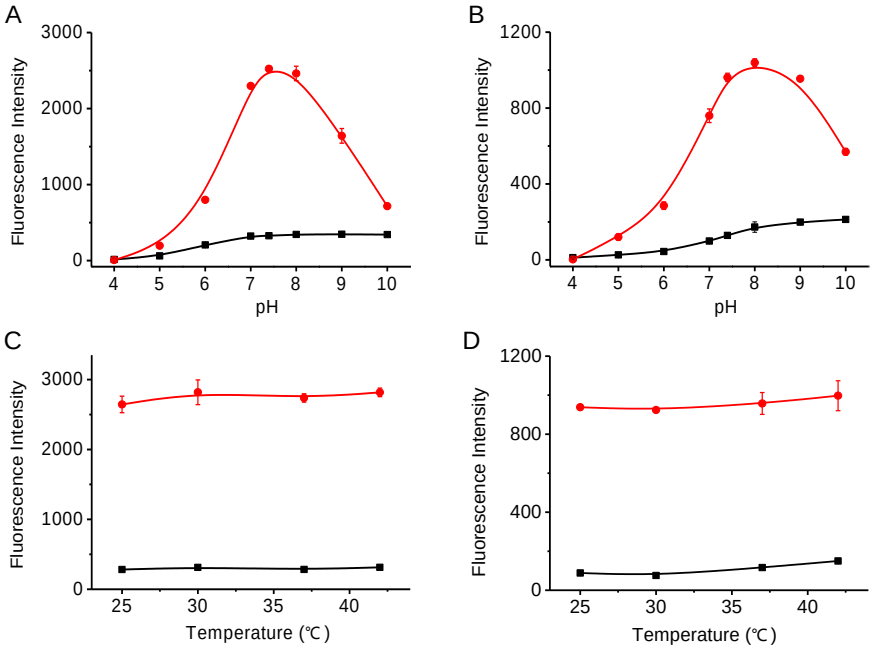

Figure S26. pH and temperature study. Effects of pH (A, B) and temperature (C, D) on the fluorescence intensity of 10 μM of NIR-II-F2LAP (A, C) and NIR-II-F3LAP (B, D) in the absence (black) or presence (red) of 25 U/L LAP. Results are the mean ± SD (n = 3).

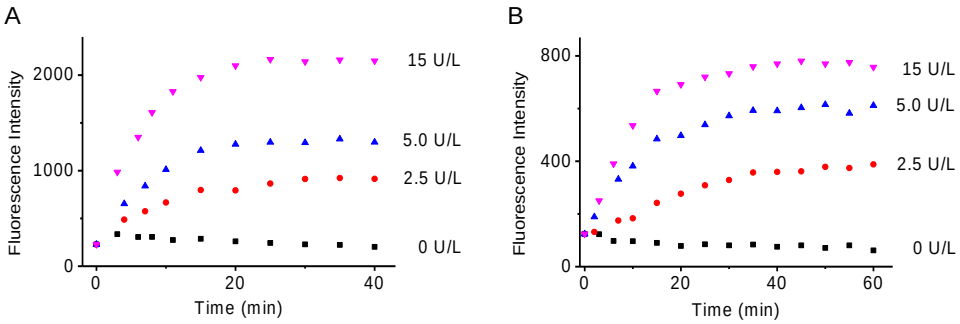

Figure S27. Effects of reaction time on the fluorescence intensity of 10 μM of NIR-II-F2LAP (A) and NIR-II-F3LAP (B) with varied LAP (0, 2.5, 5 and 15 U/L).

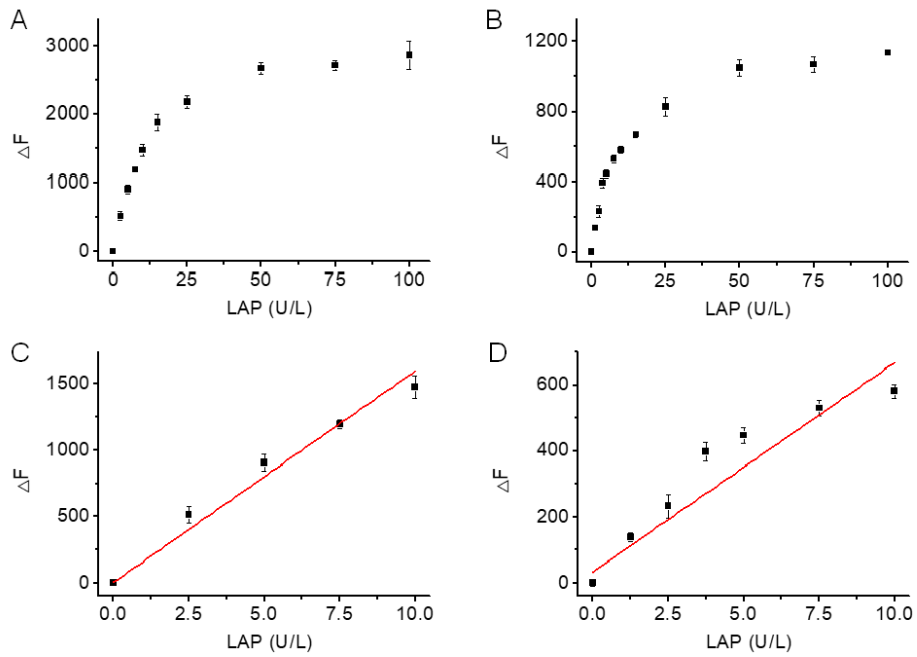

Figure S28. Fluorescence intensity of 10 μM of NIR-II-F2LAP (A) and NIR-II-F3LAP (B) versus different concentrations of LAP. Linear fluorescence enhancement of NIR-II-F2LAP (C) and NIR-II-F3LAP (D) with varied LAP. λ_{ex} = 808 nm; λ_{em} = 933 nm (NIR-II-F2LAP); λ_{em} = 1030 nm (NIR-II-F3LAP).

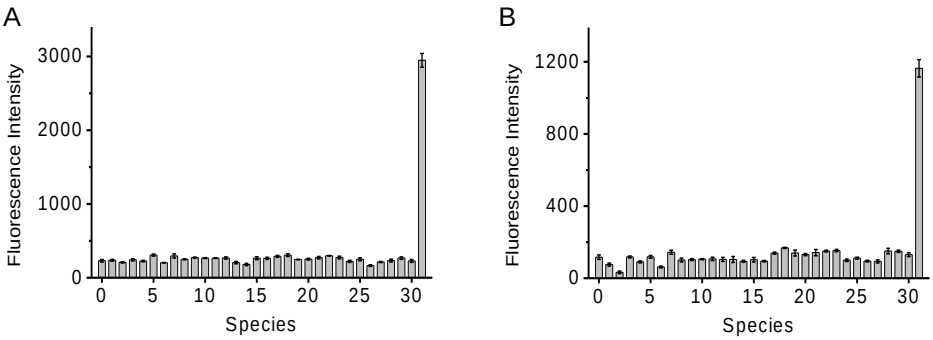

Figure S29. Fluorescence responses of 10 μM of NIR-II-F2LAP (A) and NIR-II-F3LAP (B) toward various species: (0) probe only; (1) NaCl (150 mM); (2) KCl (150 mM); (3) $CaCl_2$ (2.5 mM); (4) $MgCl_2$ (2.5 mM); (5) $ZnCl_2$ (100 μM); (6) $CuSO_4$ (100 μM); (7) $FeCl_3$ (100 μM); (8) glutamic acid (1 mM); (9) alanine (1 mM); (10) arginine (1 mM); (11) glycine (1 mM); (12) lysine (1 mM); (13) cys (1 mM); (14) GSH (1 mM); (15) vitamin C (1 mM); (16) glucose (10 mM); (17) lipase (10 μg/mL); (18) carbonic anhydrase (10 μg/mL); (19) trypsin (10 μg/mL); (20) NADPH (10 μg/mL); (21) NADH (500 μM); (22) nitroreductase (10 μg/mL); (23) carboxylesterase (0.5 U/mL); (24) H_2O_2 (100 μM); (25) HOCl (10 μM); (26) $ONOO^-$ (5 μM); (27) NaHS (100 μM); (28) alkaline phosphatase (100 U/L); (29) aminopeptidase N (20 ng/mL); (30) β-galactosidase (100 U/L); (31) LAP (100 U/L). Results are the mean ± SD (n = 3).

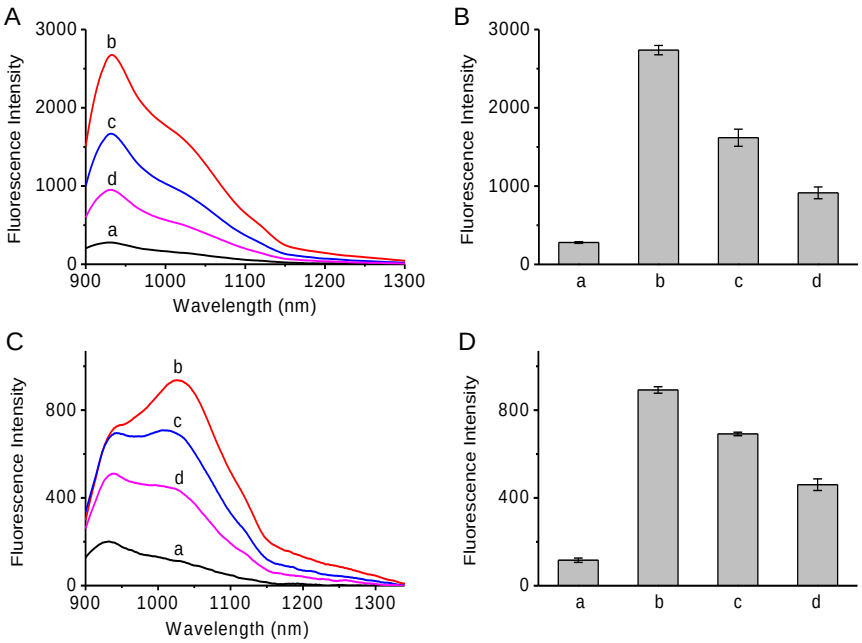

Figure S30. Effects of inhibitor bestatin on the fluorescence of 10 μM of NIR-II-F2LAP (A, B) and NIR-II-F3LAP (C, D) with 25 U/L LAP. (a) probe; (b) probe + 25 U/L LAP; (c) system b + 1 μM of bestatin; (d) system b + 2 μM of bestatin.

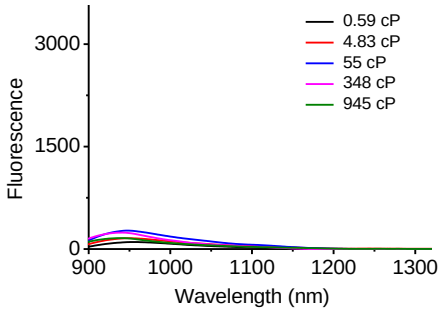

Figure S31. Fluorescence spectra of NIR-II-F2LAP (10 μM) in the mixtures of various ratios (v/v) of methanol/glycerol (the glycerol proportion from 0 to 20, 50, 80 and 99% corresponds to the viscosity of 0.59 to 4.83, 55, 348 and 945 cP, respectively; see Li *et al.*, *J. Am. Chem. Soc.*, 2019, 141, 18301-18307). λ_{ex} = 808 nm.

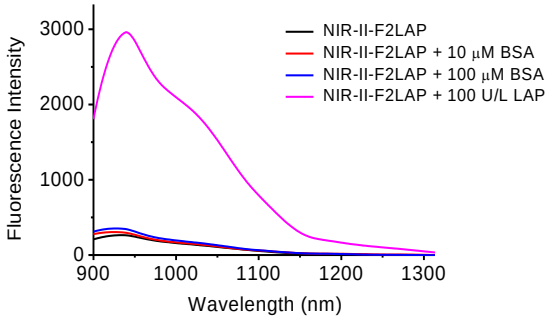

Figure S32. Fluorescence spectra of NIR-II-F2LAP (10 μM) in pH 7.4 PBS containing different analytes. λ_{ex} = 808 nm.

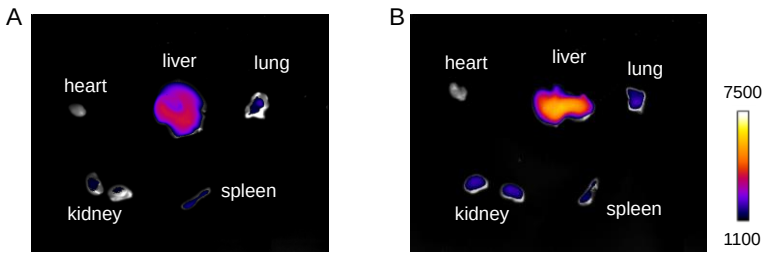

Figure S33. Fluorescence images of the dissected organs from mice treated with (A) saline or (B) 300 mg kg^{-1} APAP, followed by intravenous injection of NIR-II-F2LAP (500 μM, 200 μL). Excitation: 808 nm laser.

4. References

1. H. Y. Li, X. H. Li, X. F. Wu, W. Shi and H. M. Ma, *Anal. Chem.*, 2017, **89**, 5519-5525.
2. D. Liu, Z. He, Y. Zhao, Y. Yang, W. Shi, X. Li and H. Ma, *J. Am. Chem. Soc.*, 2021, **143**, 17136-17143.
3. O. E. Semonin, J. C. Johnson, J. M. Luther, A. G. Midgett, A. J. Nozik and M. C. Beard, *J. Phys. Chem. Lett.*, 2010, **1**, 2445-2450.
4. Q. Q. Wan, S. M. Chen, W. Shi, L. H. Li and H. M. Ma, *Angew. Chem. Int. Ed.*, 2014, **53**, 10916-10920.
5. K. V. Sashidhara, A. Kumar, M. Kumar, A. Srivastava and A. Puri, *Bioorg. Med. Chem. Lett.*, 2010, **20**, 6504-6507.